Junge, M., Wirth, R., Oberthür, T., Melcher, F., Schreiber, A. (2015): Mineralogical siting of platinum-group elements in pentlandite from the Bushveld Complex, South Africa. - *Mineralium Deposita*, *50*, 1, p. 41-54.

DOI: http://doi.org/10.1007/s00126-014-0561-0

Mineralogical siting of platinum-group elements in pentlandite from the Bushveld Complex, South Africa

Malte Junge[1], Richard Wirth[2], Thomas Oberthür[1], Frank Melcher[3], Anja Schreiber[2]

[1]Federal Institute for Geosciences and Natural Resources (BGR), Stilleweg 2, D-30655 Hannover, Germany

[2]Helmholtz Centre Potsdam, GFZ German Research Centre for Geosciences, Telegrafenberg, D-14473 Potsdam Germany

[3]Institute of Geological Sciences, University of Leoben, Peter Tunner Strasse 5, A-8700 Leoben, Austria

ABSTRACT

The Bushveld Complex in South Africa hosts the world's largest resources of platinum-group elements (PGE), which are mainly mined from three ore bodies, namely the Merensky Reef, the UG-2 chromitite and the Platreef. In these ores, the PGE are bimodally distributed, occurring both as discrete platinum-group minerals (PGM) and hosted by sulfides. The presence of PGE in sulfides has been demonstrated by electron probe microanalysis, laser ablation induced coupled plasma mass spectrometry, secondary ion mass spectrometry and particle-induced X-ray emission. However, evidence is lacking on the mineralogical siting of the PGE, e.g. whether they occur in solid solution, as nano- and/or micro-inclusions. Therefore, in the present study a combination of focused ion beam and transmission electron microscopy was used which allows to obtain crystal-structural relationships between the host mineral and incorporated trace elements and revealing the physicochemical state of the PGE in sulfides.

The present study confirms the existence of micrometer-sized discrete PGM in the ores. Further, the PGE occur in a number of forms, namely (1) as discrete nano-inclusions of PGM, (2) as patchily distributed solid solution, (3) ordered within the pentlandite crystal structure, substituting for Ni and/or Fe (superlattice), and (4) as homogenous solid solution. Nanometer-sized PGM (nPGM) show no orientation relationship with the host sulfide mineral. Consequently, they are discrete phases, which were trapped within pentlandite during sulfide growth. Heterogeneous and patchy distributions of Rh and Ir within the pentlandite lattice suggest that Rh and Ir were already present within the sulfide liquid. The absence of possible reaction partners (e.g. Bi, As, Sn) necessary for the formation of discrete PGM forced Rh and Ir to remain in the crystal lattice of pentlandite and down-temperature exsolution caused patchy distribution patterns of Rh and Ir. High concentrations of Rh and Ir in pentlandite initiate ordering of the randomly distributed PGE in form of nanometer-sized lamellae resulting in the formation of a superlattice. Palladium is homogenously distributed within the pentlandite lattice, even at high Pd concentrations, and in addition also occurs as nPGM.

INTRODUCTION

Platinum-group element (PGE) mineralization is mainly associated with mafic-ultramafic intrusions such as the Bushveld Complex in South Africa. In these ores, the PGE are usually bimodally distributed, occurring both as discrete platinum-group minerals (PGM) and hosted by sulfides. Especially pentlandite [$(Fe,Ni)_9S_8$] is known to contain elevated concentrations of Pd and Rh (e.g., Cabri and Laflamme 1981; Todd et al. 1982; Cabri et al. 1984; Oberthür et al. 1997a, 2003; Gervilla et al. 2004; Godel et al. 2007; Holwell and McDonald 2010; Osbahr et al. 2013, 2014; Junge et al. 2014).

So far, PGE contents of sulfides were studied using different analytical methods such as electron probe microanalysis (EPMA), particle-induced X-ray emission (PIXE), secondary

ion mass spectrometry (SIMS) and laser ablation induced coupled plasma mass spectrometry (LA-ICP-MS) (e.g., Cabri et al. 1984; Cabri 1988; Oberthür et al. 1997a, 2003; Osbahr et al. 2013, 2014; Junge et al. 2014). EPMA provides chemical information with detection limits of tens of ppm at a spatial resolution of about 1 µm. LA-ICP-MS enables analysis in the ppb-range but at inferior resolution due to the relative wide laser beam (10 to 50 µm). Junge et al. (2014) studied pentlandite grains from the UG-2 (Karee Mine, western Bushveld Complex, South Africa) with EPMA and LA-ICP-MS and analyzed maximum values of 2.2 wt.% Pd and 3.0 wt.% Rh (average contents in the hundreds of ppm range) and elevated contents of Ir (30 to 500 ppm), unparalleled by Os and Ru, and therefore, not reflecting inclusions of laurite [$(Ru,Os,Ir)S_2$].

Preparation of focused ion beam (FIB) foils for transmission electron microscopy (TEM) studies with applications in geosciences exists since about fifteen years (Wirth 2004, 2009). However, this technique has only occasionally been applied to problems related to ore genesis (e.g., Ciobanu et al. 2011; Wirth et al. 2013).

In the present study, pentlandite grains with elevated concentrations of PGE from the UG-2 (Karee Mine) and the Platreef (Mogalakwena Mine, Sandsloot pit) were investigated. Following ore microscopy and scanning electron microscopy (SEM) studies, high-resolution element maps and line scans were acquired using TEM in order to reveal the distribution of PGE in pentlandite on the nanometer-scale. The purpose of this study is to gather insight into the deportment of PGE in pentlandite from the Bushveld Complex and to reveal new aspects related to ore genesis.

GEOLOGICAL BACKGROUND

The Bushveld Complex in South Africa (Fig. 1) is the largest layered mafic–ultramafic intrusion on Earth covering an area of 66,000 km² and has an age of 2,055 ± 3.9 Ma (Scoates and Friedman 2008). Apart from containing the largest resources of PGE on Earth (about 70%

of the Pt and 40% of the Pd; Vermaak 1995), the Bushveld Complex also hosts economically important resources of Cr and V. Economic PGE deposits within the Bushveld Complex mainly occur in three ore bodies, namely the Merensky Reef, the UG-2 chromitite, and the Platreef. Notably, the UG-2 chromitite is the largest resource of PGE on Earth (Vermaak 1995).

The UG-2 chromitite occurs in the Upper Group of the Critical Zone, between 15 to 400 m below the Merensky Reef and has a general thickness of about one meter, varying between 0.4 and 2.5 m (e.g., Hiemstra 1979, 1985, 1986; McLaren and De Villiers 1982; Schouwstra et al. 2000). Regional studies indicate that the Merensky Reef and the UG-2 are laterally continuous over hundreds of kilometers (e.g., Von Gruenewaldt et al. 1986; Hatton and Von Gruenewaldt 1987; Scoon and Teigler 1994). In the UG-2, PGE concentrations typically range from 4 to 8 g/t and the distribution of the PGE is generally limited to the UG-2 chromitite itself, as essentially no PGE are present above or below the chromitite layer (e.g., McLaren and De Villiers 1982; Hiemstra 1985, 1986; Lee 1996; Cawthorn 2011). Copper and Ni contents are generally below 0.05 wt.%, and S is below 0.1 wt.%, indicating low sulfide contents (Von Gruenewaldt et al. 1986; Lee 1996; Cawthorn 2011). Indeed, sulfides (pentlandite, chalcopyrite and minor pyrrhotite) are rare (<1 vol.%) in the UG-2 and generally occur interstitial to chromite grains. The PGM (grain sizes <5 to 50 µm) in the UG-2 are locked within, or more commonly, occur at the peripheries of sulfide grains and the suite of PGM is dominated by laurite [RuS_2], cooperite/braggite [(Pt,Pd)S], Pt-Fe alloy and sperrylite [$PtAs_2$] (e.g., Kinloch 1982; McLaren and De Villiers 1982; Penberthy and Merkle 1999; Schouwstra et al. 2000; Kuhlmann et al. 2006; Junge et al. 2014). Platinum and the IPGE (Os, Ir, Ru) are dominantly present as discrete PGM, whereas large proportions of the Pd and Rh are hosted in pentlandite which may contain up to 2 wt.% of Pd and 3 wt.% of Rh as outlined by Junge et al. (2014).

The Platreef in the northern Bushveld Complex varies up to 400 m in thickness with sulfide contents of ca. 3 vol.% and PGE contents ranging between 1 to 4 g/t (e.g., Vermaak 1995; Kinnaird and McDonald 2005; McDonald and Holwell 2011). The floor rocks of the Platreef show lithological variation, including shale, BIF, dolomite, granite gneiss, and quartzite (e.g. Manyeruke et al. 2005; Holwell et al. 2006; McDonald and Holwell 2011). The Platreef is currently the most extensively exploited PGE deposit by open-pit mining worldwide. PGE within the Platreef are bimodally distributed, occurring both as discrete PGM and within sulfides. Again, pentlandite may hold elevated contents of PGE (Pd median values (Sandsloot; this study): 390 ppm).

SAMPLES AND ANALYTICAL TECHNIQUES

This study focuses on pentlandite from the Platreef at Mogalakwena Mine (Sandsloot pit) in the northern Bushveld Complex and from the UG-2 chromitite at the Karee Mine, western Bushveld Complex (Fig. 1). Following conventional methods of study, namely ore microscopy, scanning electron microscopy (SEM) and electron probe microanalysis (EPMA), seven electron transparent foils from three pentlandite grains of the UG-2 with the largest concentrations of Pd and Rh (Table 1), were sputtered out of one polished section (AS 8918b; Table 2). From the Platreef, eight electron transparent foils (four from AS10340, three from AS7368, and one from AS7372) were sputtered out of pentlandite with FIB. Pentlandite grains of the Platreef contain several 100s ppm of Pd (median values: Pd: 390 ppm). In total, 15 TEM foils of pentlandite were analyzed for the distribution of PGE on the nanometer-scale.

Pentlandite grains were analyzed with a CAMECA SX 100 electron microprobe using the following analytical conditions: 20 kV acceleration voltage,120 nA sample current, and up to 180 s measuring time were employed. Synthetic metals (Pd, Rh, Pt, Ag, Co, Cu, Se) and natural sulfides (pentlandite) were used as standards. Mean detection limits were 75 ppm for

Co, 100 ppm for Se, 120 ppm for Rh, 140 ppm for Pd, 160 ppm for Ag, and 300 ppm for Pt. LA-ICP-MS (laser wavelength 193 nm, Agilent 7500i) measurements were conducted using a spot size of 10 to 25 µm in diameter, a laser frequency of 20 Hz and 0.95 GW/cm², and a fluence of 4.8 J/cm². Acquisition time was 20 s for the background and 20 s for the mineral analysis. Signal quantification was carried out by GLITTER (Van Achterbergh et al. 2000). The methodology of the LA-ICP-MS is the same as described by Osbahr et al. (2013).

EPMA and LA-ICP-MS are key methods for the in situ analysis of major, minor and trace elements in geosciences. EPMA is a non-destructive method with an electron beam size down to 1 µm (analytical volume of a few cubic micrometers) emitting X-rays that are analyzed by wavelength dispersive spectrometry. Detection limits of EPMA are in the 10s to 100s ppm-range. LA-ICP-MS is a destructive method creating craters or lines of several 10s to 100s cubic micrometers in volume. The larger analytical volume obtained by LA-ICP-MS and the measurement of isotopes instead of X-rays allow analysis of trace elements in the ppb-range. Both, EPMA and LA-ICP-MS, deliver only chemical data. Time resolved spectra as obtained by LA-ICP-MS may discern very tiny inclusions when using appropriate analytical conditions, however, no direct confirmation and visualization of such inclusions are possible. In contrast, TEM allows a direct link between the crystal and its chemical composition on the nanometer-scale. The preparation of electron transparent foils for the TEM investigation was carried out using a FIB technique, which is a site-specific preparation method. For this study foils with a size of 15 x 10 x 0.15 µm were sputtered with Ga-ions accelerated to 30 keV from chosen locations within pentlandite. Electron transparent foils were cut from pentlandite grains previously analyzed by EPMA (Platreef and UG-2; see Table 1).

For the TEM study, a FEI F20 X-Twin transmission electron microscope with a Schottky field emitter as electron source was used at the GeoForschungsZentrum in Potsdam. The TEM, equipped with a Gatan Tridiem Imaging Filter, a Fishione high-angle annular dark field

detector (HAADF) allowing for Z-contrast sensitive imaging, and an EDAX X-ray analyzer (Wirth et al. 2013).

Crystallographic information of nano-crystals and host minerals were obtained from fast Fourier transforms (FFT) which have been calculated from high-resolution images (HREM). For that purpose, measured d-spacings from single crystal diffraction patterns were compared with calculated d-spacings from the literature (American Mineralogist Crystal Structure Database) by measuring the distance between Bragg reflections and the angles between the individual reflections. Chemical compositions of phases were measured with an EDX X-ray analyzer in the scanning transmission electron microscopy mode (STEM). Low Ga-concentrations in the EDX measurements of pentlandite are usually present in the EDX spectra due to Ga-ion implantation during FIB sample preparation. Detailed descriptions of the FIB sample preparation were given elsewhere (Wirth 2004, 2009; Wirth et al. 2013).

RESULTS

Geochemical data of PGE within the UG-2 (whole-rock data) are compared to PGE data of pentlandite analyzed by LA-ICP-MS (normalized to C1-chondrite; Fig. 2). The whole-rock data closely correspond to the average PGE data of the UG-2 as given by Barnes and Maier (2002). However, the chondrite-normalized pattern for the PGE in pentlandite shows a distinct fractionation (enrichment) of Rh and Pd as well as Ir. In contrast, Os, Ru, and Pt display minima. Therefore, Junge et al. (2014) proposed that the PGE-in-pentlandite pattern largely reflects the capability of pentlandite to host Rh and Pd as well as some Ir in its crystal lattice, and as Pt is not compatible in pentlandite, this element forms discrete PGM. Ruthenium and Os appear to have undergone a comparable fate as Pt as they are mainly found in laurite [RuS_2].

In samples of the UG-2 and the Platreef, discrete PGM (grain sizes ~1 to 50 µm) were detected by ore microscopy and analyzed using SEM and EPMA. The PGM in the UG-2 at

177 the Karee Mine are mainly cooperite/braggite [(Pt,Pd)S], laurite, and Pt-Fe alloy (Fig. 3A).
178 The suite of PGM is Pt- and IPGE-dominated although the whole-rock analysis of the sample
179 (Junge et al. 2014) indicates elevated contents of Pd (2290 ppb) and Rh (790 ppb). In the UG-
180 2, Pd, Rh, and Ir are hosted by base metal sulfides, whereas the concentrations of Pt, Os, and
181 Ru in base metal sulfides are low and therefore, these metals occur as discrete PGM (e.g.
182 Junge et al. 2014).

183 In polished sections from the Platreef, additionally to the identification of discrete PGM
184 (mainly Pt-Pd-bismuthotellurides, cooperite/braggite; grain sizes ~1 to 50 µm; Fig. 3B),
185 elevated concentrations of Pd (median values: Pd: 390 ppm) in pentlandite were measured
186 with EPMA. Additionally, some (Pd,Pt)-germanides [$(Pd,Pt)_2Ge$] were observed, which so far
187 have been rarely described (McLaren and De Villiers 1982, UG-2; Kozyrev et al. 2002,
188 Norilsk-Talnakh; Grokhovskaya et al. 2005, Burakovsk Layered Complex; Holwell et al.
189 2006, Platreef/Sandsloot; Subbotin et al. 2012, Fedorova-Pana).

190

191 **Nano-inclusions of PGM (nPGM) in pentlandite**

192 In addition to the occurrence of discrete PGM grains (µm-sized), the TEM studies confirm
193 the presence of heterogeneously distributed nm-sized PGM in pentlandite in the FIB foils of
194 both the UG-2 and the Platreef (Figs. 3C, D, Table 2). These nPGM are mainly idiomorphic,
195 with grain sizes <100 nm. Analyses of the nPGM display that these are Pt-Pd-Sn compounds,
196 Pt-bismuthides and Pt-tellurides (Platreef only), a Pd-Sn compound (probably atokite [Pd_3Sn];
197 UG-2 only) and Pt-(Fe,Cu) alloys (at both localities). The example shown (Fig. 3C; TEM
198 dark-field image) demonstrates that the Pt-Pd-Sn-nPGM (Platreef) is not oriented relative to
199 the crystal lattice of the host sulfide and therefore, is a discrete phase. Notably, some fluid-
200 inclusion trails were observed in pentlandite of the Platreef containing a nanometer-sized Pt-
201 telluride with a grain size of circa 50 nm (foil: #3502; Fig. 3D).

A circa one µm large Pt-(Fe,Cu) alloy (probably tulameenite, [(Pt_2FeCu]) is shown in Figure 4A (foil #3512). The diffraction pattern of this PGM is disturbed, indicated by irregular shapes of Bragg reflections especially at the higher order reflections (Fig. 4B), whereas the diffraction pattern of the surrounding pentlandite is undisturbed. Figure 4C shows element maps of the area of the PGM which reveal that Pt, Fe and Cu are homogenously distributed within the PGM.

PGE within the crystal lattice of pentlandite

Platinum-group elements within the crystal lattice of pentlandite of the UG-2 (Table 2) are substituting for Ni and/or Fe and occur as (i) patchily distributed PGE (Fig. 5A), or (ii) in an ordered arrangement forming oriented lamellar nano-structures (Fig. 6). In the Platreef samples analyzed by EDX, however, no random or ordered arrangement of PGE in pentlandite was observed (Table 2).

(i) Patchily distributions in pentlandite comprise concentrations of (Rh, Ir) in the form of small (10 to 100 nm) specks (Fig. 5A, Table 2). An EDX line profile across one single patch demonstrates that these patches represent an enrichment of Rh and Ir and simultaneous depletion of Fe and Ni (Fig. 5C). The heterogeneous and patchy distribution of Rh and Ir can also be observed in the HREM lattice fringe image of pentlandite (Fig. 5B). In this image, the dark zones are due to local enrichments of Rh and Ir, causing higher mass adsorption contrast resulting in darker contrasts in the HREM image. Element distribution maps using Pt-L and Rh-L X-ray intensities (Fig. 4C) further visualize the patchy distribution of PGE (Pt and Rh). The line scan (Fig. 5C) together with the element distribution maps (Fig. 4C) confirm that Rh and Ir are heterogeneously distributed in the pentlandite lattice. In electron diffraction patterns of the Rh- and Ir-rich zones, only the Bragg reflections of pentlandite are detectable. Note that in case that nanocrystals would be present in pentlandite, additional diffraction spots should

be observed, which is not the case. Therefore, Rh and Ir occur in solid solution and do not reflect any discrete compound or mineral.

(ii) In pentlandite grains from the UG-2 with unusually high concentration of Rh (up to 12.3 wt.%) and Pd (up to 0.6 wt.%) - (foils: #3512, #3516, #3534; Table 1), Rh and Ir occur in an ordered arrangement within the pentlandite lattice forming orientated lamellar nano-structures (Fig. 6). These lamellae, which are visible in the HREM in Figure 6C, have thicknesses of several nanometers. The lamellae and the higher contrasts are a result of the enrichment of Rh and Ir, which cause higher mass adsorption contrasts and therefore darker contrasts in the HREM image.

These lamellae follow four different orientations. Detailed analysis of these lamellae revealed that they reflect chemical variations of Rh- and Ir-rich and Ni- and Fe-poor zones (Fig. 6E). Measuring the distance between the Bragg reflections in the diffraction pattern of the lamellae and indexing the respective reflections with the calculated (hkl)-data from the American Mineralogist Crystal Structure Database demonstrates enrichments of Ir and Rh on the (111)-plane of pentlandite (Fig. 6D). Additional weak diffraction signals (streaking) between the major Bragg reflections of pentlandite caused by the presence of thin Ir- and Rh-rich lamellae on the (111)-plane are also visible in the diffraction pattern (Fig. 6D).

This periodic structure is defined as a superlattice, suggesting an ordered arrangement of Ir and Rh within the pentlandite crystal lattice. In contrast, solid solution represents random arrangements of element incorporation. The intensive study of superlattices that followed their discovery (e.g., Johansson and Linde 1925) provided an excellent base for the understanding of order-disorder transformation within a crystal.

It should be noted that the present study was sparked off by the identification by EPMA and LA-ICP-MS of elevated contents (in the %-range) of Pd and Rh in pentlandite. Nanometer-sized PGM are mainly Pt-bearing (Pt-bismuthides, Pt-tellurides, Pt-(Fe,Cu) alloys) and rarer Pd-Sn and Pt-Pd-Sn compounds. Crystal lattice related PGE concentrations

in pentlandite comprise heterogeneous and patchily distributions as well as ordered arrangements within the pentlandite lattice of Rh and Ir. Therefore, our data imply that a large proportion of the Pd is present in solid solution (substituting for Ni or Fe) in the crystal lattice of pentlandite as already suggested by e.g. Cabri et al. (1984).

DISCUSSION

State-of-the-art analytical methods, such as EPMA and LA-ICP-MS are key methods for the in situ analysis of major, minor and trace elements in modern geosciences. Analyses using EPMA and LA-ICP-MS provide information that sulfides contain PGE from the ppb to ppm range upwards. However, these methods do not allow the determination of their chemical state (PGM, nPGM, or in solid solution) in the crystal lattice. Investigation of the distribution of PGE in sulfides and the identification of discrete PGM on a nanometer-scale as well as a direct link between the crystal and its chemical composition can be obtained using the TEM. However, the draw-back of the method is the comparatively high detection limit of PGE (ca. 1,500 ppm; e.g., Wirth et al. 2013; Cabri et al. 2013).

Previous studies by EPMA and LA-ICP-MS have demonstrated that elevated concentrations of Pd and Rh may occur in pentlandite (e.g., Cabri 1984; Oberthür et al. 2003; Godel et al. 2007; Holwell and McDonald 2010; Osbahr et al. 2013, 2014; Junge et al. 2014). The association of PGE with sulfides generally points to the fact that the PGE were originally concentrated by an immiscible sulfide liquid (e.g. Naldrett et al. 1979; Naldrett 2004).

The present TEM study of samples from the UG-2 and the Platreef revealed that the PGE in pentlandite occur as discrete nPGM as well as incorporated in the crystal lattice of pentlandite, either heterogeneously distributed, or as an ordered arrangement of lamellar nano-structures. For the Platreef samples no patchy solid solution was found indicating that the PGE are homogenously distributed in pentlandite.

nPGM in pentlandite

Wirth et al. (2013) described nPGM in sulfides from the Merensky Reef. In the present study, a variety of different nPGM (Pt-bismuthides, Pt-tellurides, Pt-(Fe,Cu) alloys and rarer Pd-Sn and Pt-Pd-Sn compounds) was found in pentlandite of both the UG-2 and the Platreef (Table 2). These nPGM are idiomorphic and their crystallographic orientation is not linked to that of the pentlandite lattice, probably indicating that the nPGM crystallized earlier than pentlandite and are not results of exsolution from pentlandite. The presence of discrete micro- to nanometer inclusions of PGM was already assumed due to distinct parallel peaks of PGE and semimetals in time-resolved analysis (TRA) spectra from LA-ICP-MS studies on Platreef samples (e.g., Holwell and McDonald 2007; Hutchinson and McDonald 2008; Holwell and McDonald 2010). However, TRA spectra cannot directly distinguish between discrete micro- or nano-inclusions and heterogeneously distributed PGE occurring as solid solution. Definitely, in both the UG-2 and the Platreef a continuum of discrete micrometer-sized PGM to nPGM is present.

Patchy solid solution distribution of PGE in pentlandite

Rhodium and Ir were not detected in the form of discrete minerals, but are heterogeneously and patchily distributed within pentlandite, as indicated by element maps (Fig. 4C), electron diffraction patterns (Fig. 5B) and by line scans (Fig. 5C). Similar distribution patterns of gold in sulfides and sulfarsenides were reported by Cabri et al. (1989), Oberthür et al. (1997b) and Genkin et al. (1998). It is well known that Rh preferentially forms discrete PGM like hollingworthite [RhAsS] in chromitite (e.g., Merkle 1992) or sulfide environments (e.g., Mostert et al. 1982; Oberthür et al. 2003) in case that sufficient quantities of As and S are available in the system.

Mungall et al. (2005) demonstrated that in S-rich systems IPGE and Rh are highly compatible in monosulfide solid solution (MSS). MSS is the first phase which crystallizes from a sulfide liquid, and intermediate solid solution (ISS) crystallizes subsequently from the remaining liquid (e.g., Li et al. 1996; Mungall et al. 2005). Some authors postulate that all PGE are primarily collected by sulfide liquid in the magmatic stage due to their high partition coefficients in favor of sulfide (e.g., Campbell et al. 1983; Mungall and Naldrett 2008). Within the sulfide liquid, the PGE may be trapped as single atoms, ions, metal clusters or precursors of nPGM (Tredoux et al. 1995). Down temperature, MSS recrystallizes and since Ir and Rh are more compatible in MSS than Pd and Pt, Ir and Rh are concentrated in MSS, whereas Pd and Pt remain in the Cu-rich sulfide liquid (e.g. Mungall et al. 2005).

The heterogeneous and patchy distribution of Rh and Ir in the pentlandite lattice possibly indicates that clusters of Rh and Ir were heterogeneously distributed within the initial sulfide liquid, at magmatic temperatures, or that Rh/Ir accumulations exsolved down temperature. The absence of possible reaction partners (e.g. Bi, Te, As, Sn) necessary for the formation of discrete PGM apparently forced Rh and Ir to remain in the crystal lattice of pentlandite.

Lamellar intergrowths of PGE in pentlandite

Lamellar nano-structures were found within pentlandite from the UG-2. The thicknesses of these lamellae are only several nanometers (Fig. 6C). EDX analyses demonstrate that these structures represent Ir- and Rh-rich and relative Ni- and Fe-poor zones (Fig. 6E). Studying the diffraction pattern of these lamellae shows the presence of additional Bragg reflections besides the regular ones of pentlandite (Fig. 6D).

In general, in crystals with a disordered arrangement of atoms, crystallographically equivalent planes of atoms are statistically identical with one another. However, in a superlattice structure the distance between identical planes may be twice (or manifold) the distance between identical planes of the disordered crystal causing additional Bragg

329 reflections in the diffractions patters. This is visible in the diffraction patterns of the Ir- and
330 Rh-rich lamellae (Fig. 6D). Detailed examination revealed that these Ir- and Rh-rich zones
331 occur on the (111)-plane of pentlandite. Between the (111)-spots, at least one additional
332 diffraction spot is visible that represents a d-spacing of [2 x d_{111}] = 11.4308 Å. Streaking is
333 due to the narrow thickness of the lamellae. Due to the cubic lattice of pentlandite and the
334 fourfold-axis, four different orientations of (111)-planes exist and lamellae may show four
335 different orientation patterns within pentlandite.

336 For example, in the Cu-Au system, Cu and Au are randomly distributed in the temperature
337 range between ca. 890 and 410°C. At temperatures below 410°C, Cu and Au atoms start to
338 order along particular lattice planes, thereby creating ordered superlattices (Toth and Sato
339 1962; Barrett and Massalski 1980). Superlattices initiate near the compositions Cu_3Au, CuAu,
340 and $CuAu_3$. For the Cu-Au system (face-centered cubic crystal system) alloys containing 25
341 at.% Au (Cu_3Au), Au and Cu are randomly distributed on the cube corners or the face centers
342 at high temperatures. Below a critical temperature of 390°C, ordering takes place and Au
343 atoms are occupying the cube corners and Cu atoms the face centers (Toth and Sato 1962;
344 Barrett and Massalski 1980). The disorder-order-change, therefore, results in an additional
345 symmetry element, which causes additional Bragg reflections in the electron diffraction
346 patterns. Increasing the concentrations of Au to a composition close to Cu_3Au initiates
347 ordering of the randomly distributed Au and Cu atoms to an ordered arrangement leading to
348 the formation of a superlattice.

349 In pentlandite grains containing PGE concentrations in the range of some hundreds of ppm,
350 Rh and Ir appear to be distributed in a statistically random manner within the crystal lattice
351 and no preferred atom sites are occupied by Rh and Ir. However, with increasing
352 concentrations of Rh and Ir (at least 12.3 wt.% Rh and up to 0.6 wt.% Pd), ordering takes
353 place and certain lattice sites are preferentially occupied by only one kind of atom, causing a

change in the crystal symmetry of pentlandite, which is visible in the electron diffraction patterns.

In general, the substitution of trace elements into a solid phase is considered to be controlled by the nature of the bonding, the size of the lattice site, and the charge balance. The pentlandite structure represents a pseudo cubic closest-packing with cations (Fe, Ni) occupying the octahedral and tetrahedral sites (Rajamani and Prewitt 1973, 1975). The ionic radii (in Å) of Pd, Fe, and Ni are: $^{IV}Pd^{2+}$ = 0.64, $^{IV}Fe^{2+}$ = 0.63, and $^{IV}Ni^{2+}$ = 0.55 (Shannon 1976) thereby allowing substitution of Pd for Ni and/or Fe as the ionic radii differ by less than 15% (Goldschmidt 1926). The same is true for $^{VI}Rh^{3+}$ = 0.665, $^{VI}Ir^{3+}$ = 0.68, $^{VI}Ni^{2+}$ = 0.69, $^{VI}Fe^{2+}$ = 0.61. The electron configurations of Fe, Os, Ir, Ru and Rh have a d^2sp^3 preferred hybridization state, suitable for octahedral sites (Evans 1966; Barnes et al. 2001). Iron is consequently preferentially substituted by Os, Ir, Ru and Rh. Platinum, Pd and Ni prefer dsp^2 configurations, being suitable for the square planar sites.

Crystal growth of PGM andprecursors (PGM embryos)

A Pt-(Fe,Cu) alloy with a slightly distorted diffraction pattern indicated by smeared-out Bragg reflections visible at the higher order reflections is depicted in Figure 4B. The coalescence of "embryos" or precursors forming nanometer- to micrometer-sized crystals with minute misorientations at the interfaces causes a slightly disturbed diffraction pattern (e.g., Penn and Banfield 1998). In situ experiments have shown that many minerals are preceded by crystalline nanometer-sized particles and non-crystalline nano-phases in low temperature aqueous solution. Helmy et al. (2013) demonstrated in their high temperature experiments in the Pt-As system that this also applies for PGE in magmatic systems. These authors showed that Pt and As self-organize to nano-particles long before the melt had reached Pt-As concentrations sufficient to crystallize and form discrete PGM. The particular Pt-(Fe,Cu) alloy

of the present study (Fig. 4A) may thus represent embryos or precursor phases of PGM that coalesced as described by Helmy et al. (2013).

Teng (2013) reviewed theories of crystal formation and pointed to alternative, cluster-based pathways for crystallization, i.e. aggregation of nanometer-sized clusters, which formed crystalline structures under either an ordered or in initially random patterns (e.g., Banfield et al. 2000; Navrotsky 2004; Gebauer et al. 2008; Pouget et al. 2009; Baumgartner et al. 2013). The above hypothesis challenges the classic theory of thermodynamics and atomic structures of crystal surfaces, i.e. that crystallization is a sequential addition of atoms or ions. Penn and Banfield (1998) further described the process of crystal growth as a result of oriented nano-crystal attachment. The diffraction pattern of the Pt-(Fe,Cu) alloy (Figure 4B) supports the hypothesis of the latter authors, whereby nPGM coalesces with small misorientations causing smeared-out Bragg reflections at higher order in the diffraction pattern.

CONCLUSIONS

The presence of PGE in sulfides is known from EPMA and LA-ICP-MS studies. The present work applied conventional and follow-up high-resolution methods using combined techniques of FIB and TEM to pentlandite from both the UG-2 chromitite and the Platreef. The results indicate that, a continuum exists from discrete micrometer to nanometer-sized PGM in both the UG-2 and the Platreef. Further, Pd is present as homogenous solid solution in pentlandite. Additionally, in the UG-2 sample, Rh and Ir occur as a patchily distributed solid solution and ordered within the pentlandite crystal structure, substituting for Ni and/or Fe. The major findings of this study are:

1. In the UG-2 samples, the suite of discrete PGM mainly consists of cooperite/braggite, laurite, and Pt-Fe alloy. In the Platreef samples, discrete PGM are mainly Pt-Pd-bismuthotellurides and cooperite/braggite.

2. Within pentlandite, a variety of nanometer-sized PGM (Pt-bismuthides, Pt-tellurides, Pt-(Fe,Cu) alloy, Pd-Sn and Pt-Pd-Sn compounds) was detected. These nPGM do not display any orientation relationship to the host sulfide and therefore, probably represent discrete phases which were trapped early during pentlandite growth.
3. The heterogeneous and patchy distributions of Rh and Ir in the pentlandite lattice indicate that Rh and Ir were collected early by a sulfide liquid. The absence of possible reaction partners (e.g. Bi, As, Sn), necessary for the formation of discrete PGM, forced Rh and Ir to remain in the crystal lattice of pentlandite and their down-temperature exsolution caused patchy distribution patterns of Rh and Ir.
4. In pentlandite grains from the UG-2 with unusually high concentration of Rh (up to 12.3 wt.%) and Pd (up to 0.6 wt.%), ordering of Rh and Ir within the pentlandite lattice takes place on the (111)-plane, forming a superlattice. The lamellae show that above a certain concentration of Rh and Ir (at least 12.3 wt.% Rh and 0.6 wt.% Pd), Rh and Ir form an ordered arrangement in the pentlandite lattice, causing a change in the crystal symmetry of pentlandite.
5. Slightly disturbed diffraction patterns indicated by diffuse Bragg reflections visible at the higher order reflections of a Pt-(Fe,Cu) alloy indicate that the formation of PGM may result from embryos or precursor phases which may coalescence to form discrete PGM.
6. Our data imply that a large proportion of the Pd, even at elevated concentrations, is present in homogenous solid solution in the crystal lattice of pentlandite.

Acknowledgements

Excellent polished sections were prepared by Peter Rendschmidt, SEM studies were kindly supported by Detlef Klosa, and electron probe microanalysis was ably performed by Jerzy

Lodziak, Christian Wöhrl and Simon Goldmann, all at the BGR in Hannover. Many thanks to Helene Brätz, University of Erlangen, for carrying out the LA-ICP-MS analyses.

REFERENCES

Banfield JF, Welch SA, Zhang H, Ebert TT, Penn RL (2000) Aggregation-based crystal growth and microstructure development in natural iron oxyhydroxide biomineralization products. Science 289:751-754

Barnes S-J, Maier WD (2002) Platinum-group element distributions in the Rustenburg Layered Suite of the Bushveld Complex, South Africa. In Cabri LJ (ed) The Geology, Geochemistry, Mineralogy and Mineral Beneficiation of Platinum-Group Elements, Special Volume 54 Canadian Institute of Mining, Metallurgy and Petroleum pp 431-458

Barnes S-J, Van Achterbergh E, Makovicky E, Li C (2001) Proton microprobe results of partitioning of platinum-group elements between monosulphide solid solution and sulphide liquid. S Afr J Geol 104:275-286

Barrett C, Massalski TB (1980) Structure of Metals. International Series on Materials Science and Technology, Oxford

Baumgartner J, Dey A, Bomans PHH, Le Coadou C, Frantzl P, Sommerdijk NAJM, Faivre D (2013) Nucleation and growth of magnetite from solution. Nature Materials 12:310-314

Cabri LJ (1988) Applications of proton and nuclear microprobes in ore deposit mineralogy and metallurgy. Nucl. Instr. & Methods in Physics Research 30:459-465

Cabri LJ, Laflamme JHG (1981) Analyses of minerals containing platinum-group elements. In Cabri LJ (ed) Platinum-Group elements: Mineralogy, Geology, Recovery, CIM Special Volume 23, pp 151-173, 2nd edition reprinted 1989

Cabri LJ, Blank H, El Goresy A, Laflamme JHG, Nobiling R, Sizgoric MB, Traxel K (1984) Quantitative trace-element analyses of sulfides from Sudbury and Stillwater by Proton Microprobe. Can Mineral 22:521-542

Cabri LJ, Chryssoulis SL, De Villiers JPR, Laflamme JHG, Buseck PR (1989) The nature of "invisible" gold in arsenopyrite. Can Min 27:353-362

Cabri LJ (2013) Nanometer-sized platinum-group minerals (PGM) in base metal sulfides: new evidence for an orthomagmatic origin of the Merensky Reef PGE ore deposit, Bushveld Complex, South Africa: Discussion. Can Mineral 49:817-819

Campbell IH, Naldrett AJ, Barnes S-J (1983) A Model for the Origin of the Platinum-Rich Sulfide Horizons in the Bushveld and Stillwater Complexes. J Petrol 24:133-165

463 Cawthorn RG (2011) Geological investigations from the PGE distribution in the Bushveld
464 Merensky and UG2 chromite reefs. J S Afr I Min Metall 111:67-79

465 Ciobanu CL , Cook NJ, Utsunomiya S, Pring A, Green L (2011) Focussed ion beam-
466 transmission electron microscopy application in ore mineralogy: Bridging micro- and
467 nanoscale observations. Ore Geol Rev 42:6-31

468 Evans RC (1966) An introduction to crystal chemistry. University Printing Home, Cambridge

469 Gebauer D, Volkel A, Cölfen H (2008) Stable prenucleation calcium carbonate clusters.
470 Science 322:1819-1822

471 Genkin AD, Bortnikov NS, Cabri LJ, Wagner FE, Stanley CJ, Safonov YG, McHahon G,
472 Friedl J, Kerzin AL, Gamyanin GN (1998) A multidisciplinary study of invisible gold in
473 arsenopyrite from four mesothermal gold deposits in Siberia, Russian Federation. Econ
474 Geol 93:463-487

475 Gervilla F, Cabri LJ, Kojonen K, Oberthür T, Weiser T, Johanson B, Sie SH, Campbell JL,
476 Teesdale WJ, Laflamme JHG (2004) Platinum-Group Element Distribution in Some Ore
477 Deposits: Results of EPMA and Micro-PIXE analyses. Microchimica Acta 147:167-173

478 Godel B, Barnes S-J, Maier WD (2007) Platinum-Group Elements in Sulphide Minerals,
479 Platinum-Group Minerals, and Whole-Rocks of the Merensky Reef (Bushveld Complex,
480 South Africa): Implications for the Formation of the Reef. J Petrol 48:1569-1604

481 Goldschmidt VM (1926) Geochemische Verteilungsgesetze der Elemente – VII Die Gesetze
482 der Kristallochemie. Skrifter utgitt av det Norske Videnskaps Akademi i Oslo, 1:
483 Matematisk - naturvidenskapelig klasse, University of Oslo

484 Grokhovskaya TL, Lapina MI, Ganin VA, Grinevich NG (2005) PGE Mineralization in the
485 Burakovsk Layered Complex, Southern Karelia, Russia. Geol Ore Deposits 47:283-308

486 Hatton CJ, Von Gruenewaldt G (1987) The geological setting and petrogenesis of the
487 Bushveld chromitite layers. In Stowe CW (ed) Evolution of Chromium Ore Fields. Van
488 Nostrand Reinhold, United States of America

489 Helmy H, Ballhaus C, Wirth R (2013) Noble metal nanoclusters and nanoparticles precede
490 mineral formation in magmatic sulphide melts. Nature communications 4:1-7

491 Hiemstra SA (1979) The role of collectors in the formation of platinum deposits in the
492 Bushveld. Can Mineral 17:469-482

493 Hiemstra SA (1985) The Distribution of Some Platinum-Group Elements in the UG-2
494 Chromitite Layer of the Bushveld Complex. Econ Geol 80:944-957

495 Hiemstra SA (1986) The Distribution of Chalcophile and Platinum-Group Elements in the
496 UG-2 Chromitite Layer of the Bushveld Complex. Econ Geol 81:1080-1086

497 Holwell DA, McDonald I (2007) Distribution of platinum-group elements in the Platreef at
498 Overysel, northern Bushveld Complex: a combined PGM and LA-ICP-MS study. Contrib
499 Mineral Petr 154:171-190

500 Holwell DA, McDonald I (2010) A Review of the Behavior of Platinum Group Elements
501 within Natural Magmatic Sulfide Ore Systems. Platinum Metals Review 54:26-36

502 Holwell DA, McDonald I, Armitage PEB (2006) Platinum-group mineral assemblages in the
503 Platreef at the Sandsloot Mine, northern Bushveld Complex, South Africa. Mineral Mag
504 70:83-101

505 Hutchinson D, McDonald I (2008) Laser ablation ICP-MS study of platinum-group elements
506 in sulphides from the Platreef at Turfspruit, northern limb of the Bushveld Complex, South
507 Africa. Miner Depos 43:695-711

508 Johansson CH, Linde JO (1925) Röntgenographische Bestimmung der Atomanordnung in den
509 Mischkristallreihen Au-Cu und Pd-Cu. Annalen der Physik 383:439-460

510 Junge M, Oberthür T, Melcher F (2014) Cryptic variation of chromite chemistry, platinum-
511 group element and platinum-group mineral distribution in the UG-2 chromitite: An
512 example from the Karee Mine, western Bushveld Complex, South Africa. Econ Geol
513 109:795-810

514 Kinloch ED (1982) Regional Trends in the Platinum-Group Mineralogy of the Critical Zone
515 of the Bushveld Complex, South Africa. Econ Geol 77:1328-1347

516 Kinnaird JA, McDonald I (2005) An introduction to mineralization in the northern limb of the
517 Bushveld Complex. Applied Earth Science (Trans. Inst. Min. Metall. B) 114:B194–B198

518 Kozyrev SM, Komarova MZ, Emelina LN, Oleshkevich OI, Yakovleva OA, Lyalimov DM,
519 Maximov VI (2002) The mineralogy and behavior of PGM during processing of the
520 Noril'sk-Talnakh PGE-Cu-Ni ores. In Cabri LJ (ed) The Geology, Geochemistry,
521 Mineralogy and Mineral Beneficiation of Platinum-Group Elements, Special Volume 54
522 Canadian Institute of Mining, Metallurgy and Petroleum pp 757-791

Kuhlmann G, Oberthür T, Melcher F, Lodziak J, (2006) UG2 Chromititthorizont – Mineralogisch-Geochemische Feinstratigraphie, Schwerpunkt Platinmetall-Verteilung. Bundesanstalt für Geowissenschaften und Rohstoffe (BGR), Internal Report Tgb.-Nr. 11327/06

Lee CA (1996) A Review of Mineralization in the Bushveld Complex and some other Layered Intrusions. In Cawthorn RG (ed) Layered Intrusions. Elsevier, pp. 103-145

Li C, Barnes S-J, Makovicky E, Rose-Hansen J, Makovicky M (1996) Partitioning of nickel, copper, iridium, rhenium, platinum, and palladium between monosulfide solid solution and sulfide liquid: Effects of composition and temperature. Geochm Cosmochim Ac 60:1231-1238

Manyeruke TD, Maier WD, Barnes S-J (2005) Major and trace element geochemistry of the Platreef on the farm Townlands, northern Bushveld Complex. S Afr J Geol 108:381-396

McDonald I, Holwell D (2011) Geology of the Northern Bushveld Complex and the Setting and Genesis of the Platreef Ni-Cu-PGE Deposit. In Li C, Ripley E (eds) Magamtic Ni-Cu and PGE deposits: geology, geochemistry, and genesis. Rev Econ Geol. v. 17, pp. 297–327

McDonough WF, Sun S.-s (1995) The composition of the Earth. Chem Geol 120:223-253

McLaren CH, De Villiers JPR (1982) The Platinum-Group Chemistry and Mineralogy of the UG-2 Chromitite Layer of the Bushveld Complex. Econ Geol 77:1348-1366

Merkle RKW (1992) Platinum-group minerals in the middle group of chromitite layers at Marikana, western Bushveld Complex: indications for collection mechanism and postmagmatic modification. Can J Earth Sci 29:209-221

Mostert AB, Hofmeyr PK, Potgieter GA (1982) The platinum-group mineralogy of the Merensky Reef at Impala Platinum Mines, Bophutatswana. Econ Geol 77:1385–1394

Mungall J, Naldrett AJ (2008) Ore deposits of the platinum-group elements. Elements 4:253-258

Mungall J, Andrews D, Cabri L, Sylvester P, Tubrett M (2005) Partitioning of Cu, Ni, Au, and platinum-group elements between monosulfide solid solution and sulfie melt under controlled oxygen and sulfur fugacity. Geochm Cosmochim Ac 69:4349-4360

Naldrett AJ (2004) Magmatic Sulfide Deposits. Springer, Heidelberg

552 Naldrett AJ, Hoffman EL, Green AH, Chen-Lin Chou, Naldrett SR (1979) The composition of
553 Ni-sulfide ores, with particular reference to their content of PGE and Au. Can Mineral
554 17:403-415

555 Navrotsky A (2004) Energetic clues to pathways to biomineralization: Precursors, clusters,
556 and nanoparticles. Proceedings of the National Academy of Sciences 101:12096-12101

557 Oberthür T, Cabri LJ, Weiser T, McMahon G, Müller P (1997a) Pt, Pd and other trace
558 elements in sulfides of the Main Sulfide Zone, Great Dyke, Zimbabwe – a reconnaissance
559 study. Can Mineral 35:597-609

560 Oberthür T, Weiser T, Amanor JA, Chryssoulis SL (1997b) Mineralogical siting and
561 distribution of gold in quartz veins and sulfide ores of the Ashanti mine and other deposits
562 in the Ashanti belt of Ghana: genetic implications. Miner Depos 32:2-15

563 Oberthür T, Weiser T, Gast L, Kojonen K (2003) Geochemistry and mineralogy of platinum-
564 group elements at Hartley Platinum Mine, Zimbabwe. Miner Depos 38:327-343

565 Osbahr I, Klemd R, Oberthür T, Brätz H, Schouwstra R (2013) Platinum-group element
566 distribution in base-metal sulfides of the Merensky Reef from the eastern and western
567 Bushveld Complex, South Africa. Miner Depos 48:211-232

568 Osbahr I, Oberthür T, Klemd R, Josties A (2014) Platinum-group element distribution in base-
569 metal sulfides of the UG2 chromitite, Bushveld Complex, South Africa – a reconnaissance
570 study. Miner Depos 49:655-665

571 Penberthy CJ, Merkle RKW (1999) Lateral variations in the platinum-group element content
572 and mineralogy of the UG2 Chromitite Layer, Bushveld Complex. S Afr J Geol 102:240-
573 250

574 Penn RL, Banfield JF (1998) Imperfect Oriented Attachment: Dislocation Generation in
575 Defect-Free Nanocrystals. Science 281: 969-971

576 Pouget EM, Bomans PHH, Goosl JACM, Frederik PM, de With G, Sommerdijk NAJM
577 (2009) The initial stages of template-controlled $CaCO_3$ formation revealed by cryo-TEM.
578 Science 323:1455-1458

579 Rajamani V, Prewitt CT (1973) Crystal Chemistry of Natural Pentlandites. Can Mineral
580 60:39-48

581 Rajamani V, Prewitt CT (1975) Thermal Expansion of the Pentlandite Structure. Am Mineral
582 60:39-48

583 Scoates JS, Friedman RM (2008) Precise age of the platiniferous Merensky Reef, Bushveld
584 Complex, South Africa, by the U-Pb Zircon chemical abrasion ID-TIMS technique. Econ
585 Geol 103:465-471

586 Scoon RN, Teigler B (1994) Platinum-Group Element Mineralization in the Critical Zone of
587 the Western Bushveld Complex: I. Sulfide Poor-Chromitites below the UG-2. Econ Geol
588 89:1094-1121

589 Schouwstra R, Kinloch E, Lee C (2000) A short review of the Bushveld Complex. Platinum
590 Minerals Review 44:33-39

591 Shannon RD (1976) Revised Effective Ionic Radii and Systematic Studies of Interatomic
592 Distances in Halides and Chalcogenides. Acta Crystallogr 32:751-767

593 Subbotin VV, Korchagin AU, Savchenko EE (2012) Platinum mineralization of the Fedorova-
594 Pana ore node: types of ores, mineral compositions and genetic features. Vestnick of the
595 Kola Science Center of the Russian Academy of Sciences, Apatity, l:54-65 (in Russian)

596 Teng HH (2013) How ions and molecules organize to form crystals. Elements 9:189-194

597 Todd SG, Keith DW, Le Roy LW, Schissel DJ, Mann EL, Irvine TN (1982) The J-M
598 platinum-palladium reef of the Stillwater Complex, Montana: I. Stratigraphy and
599 petrology. Econ Geol 77:1454-1480

600 Toth RS, Sato H (1962) Long period superlattice Cu_3Au II. J Appl Phys 33:3250-3256

601 Tredoux M, Lindsay NM, Davies G, McDonald I (1995) The fractionation of platinum-group
602 elements in magmatic systems, with the suggestion of a novel causal mechanism. S Afr J
603 Geol 98:157-167

604 Vermaak C (1995) The Platinum-Group Metals - A global perspective. Mintek

605 Von Gruenewaldt G, Hatton CJ, Merkle RKW, Gain SB (1986) Platinum-Group Element-
606 Chromite Associations in the Bushveld Complex. Econ Geol 81:1067-1079

607 Wirth R (2004) Focused Ion Beam (FIB): A novel technology for advanced application of
608 micro- and nanoanalysis in geosciences and applied mineralogy. Eur J Mineral 16:863-876

609 Wirth R (2009) Focused Ion Beam (FIB) combined with SEM and TEM: Advanced analytical
610 tools for studies of chemical composition, microstructure and crystal structure in
611 geomaterials on a nanometer scale. Chem Geol 261:217-229

612 Wirth R, Reid D, Schreiber A (2013) Nanometer-sized platinum-group minerals (PGM) in
613 base metal sulfides: New evidence for an orthomagmatic origin of the Merensky Reef PGE
614 ore deposit, Bushveld Complex, South Africa. Can Mineral 51:143-155

615

616

Figure caption:

Fig. 1: Geological map of the Bushveld Complex with sample locations of the UG-2 chromitite (Karee Mine) and the Platreef (Sandsloot, Mogalakwena Mine).

Fig. 2: Chondrite-normalized PGE distributions of average UG-2 of the western Bushveld (Barnes & Maier, 2002; stippled line), of DO-24 from the Karee Mine (Junge et al. 2014) whole rock data (red). PGE contents of pentlandite analyzed by LA-ICP-MS (range in blue). C1-chondrite values from McDonough and Sun (1995).

Fig. 3 A: Chalcopyrite (1), pentlandite (2), millerite (3), pyrite (4), braggite [(Pt,Pd)S] (5), kotulskite [PdTe] (6), temagamite [Pd_3HgTe_3] (7) (UG-2, Lebowa Mine, Eastern Bushveld Complex; AS7631, from Kuhlmann et al. 2006). B: Pyrrhotite, pentlandite and chalcopyrite with PGE-bismuthotelluride (white) in reflected light, in oil (Platreef, Mogalakwena Mine; AS10451). C: TEM bright-field image of one inclusion of a discrete nPGM [(Pt,Pd)Sn] in pentlandite of the Platreef (foil: #3504). D: Discrete nPGM [PtTe] within fluid inclusions trail (Platreef, foil: #3502).

Fig. 4 A: TEM bright-field image of an inclusion of Pt-(Fe,Cu) in pentlandite (UG-2, foil #3512). B: Electron diffraction pattern of the Pt-(Fe,Cu) showing disturbed Bragg reflections at higher order (UG-2, foil #3512). C: Element maps showing the distributions of Pt, Rh, Cu, Ni and Fe and the chemistry of patches (bright gray) in pentlandite (dark gray) and of the Pt(Fe,Cu) alloy (white) in foil #3512.

Fig. 5: A: Patches of Ir- and Rh-rich zones (white) in „normal“ pentlandite (gray) (foil #3514). B: HREM of patchy distribution of PGE in pentlandite (foil #3516). C: EDX-line scan (orange line) showing the distribution of Ir, Rh, Ni, and Fe (foil #3516).

Fig. 6: Lamellar structures of pentlandite (foil # 3516). A and B: Structures in TEM mode. C: HREM image of lamellae D: FFT image of C. Note additional reflections indicating the presence of a superlattice. E: line scan (red line) through lamellae.

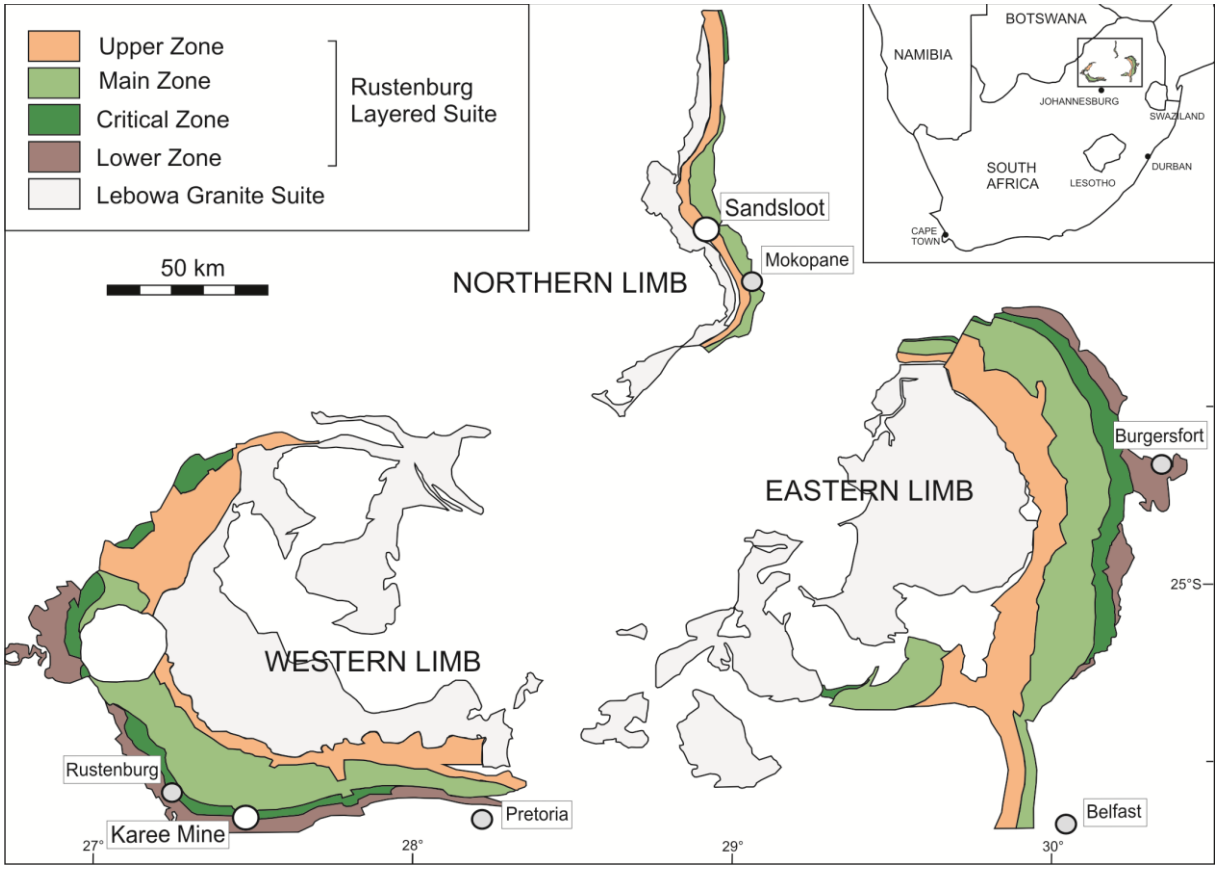
Upper Zone
Main Zone
Critical Zone
Lower Zone
Lebowa Granite Suite
Rustenburg Layered Suite
50 km
NORTHERN LIMB
EASTERN LIMB
WESTERN LIMB
Sandsloot
Mokopane
Burgersfort
Rustenburg
Karee Mine
Pretoria
Belfast
25°S
27°
28°
29°
30°
BOTSWANA
NAMIBIA
JOHANNESBURG
SWAZILAND
SOUTH AFRICA
LESOTHO
DURBAN
CAPE TOWN

Fig 1

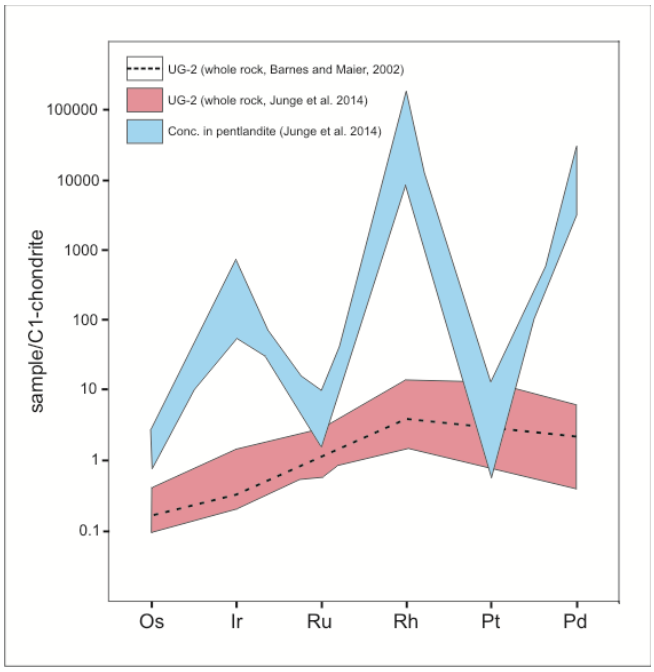

653

654

655 Fig 2

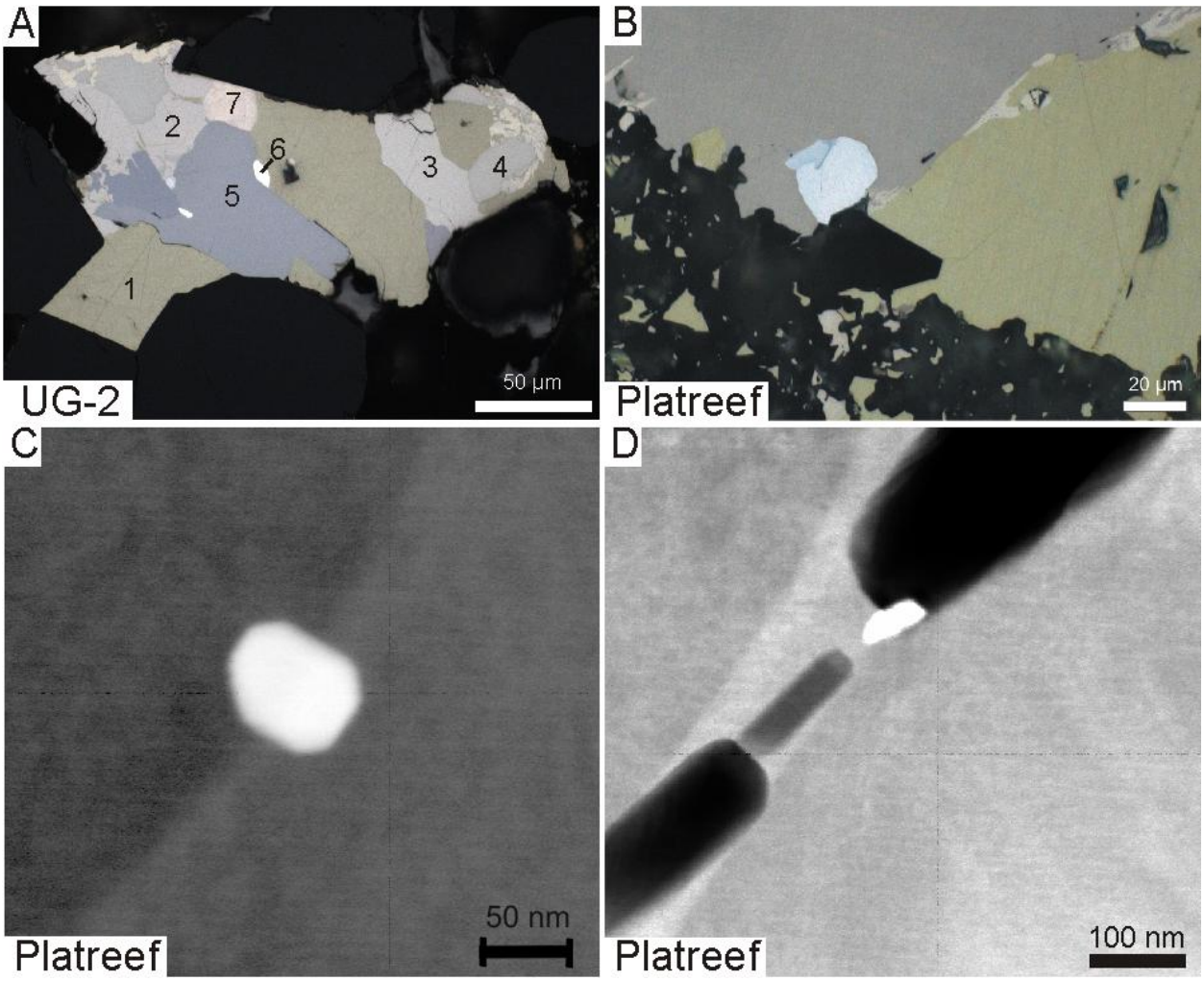
A
7
2
6
3
4
5
1
50 µm
UG-2
B
20 µm
Platreef
C
50 nm
Platreef
D
100 nm
Platreef

Fig 3

660

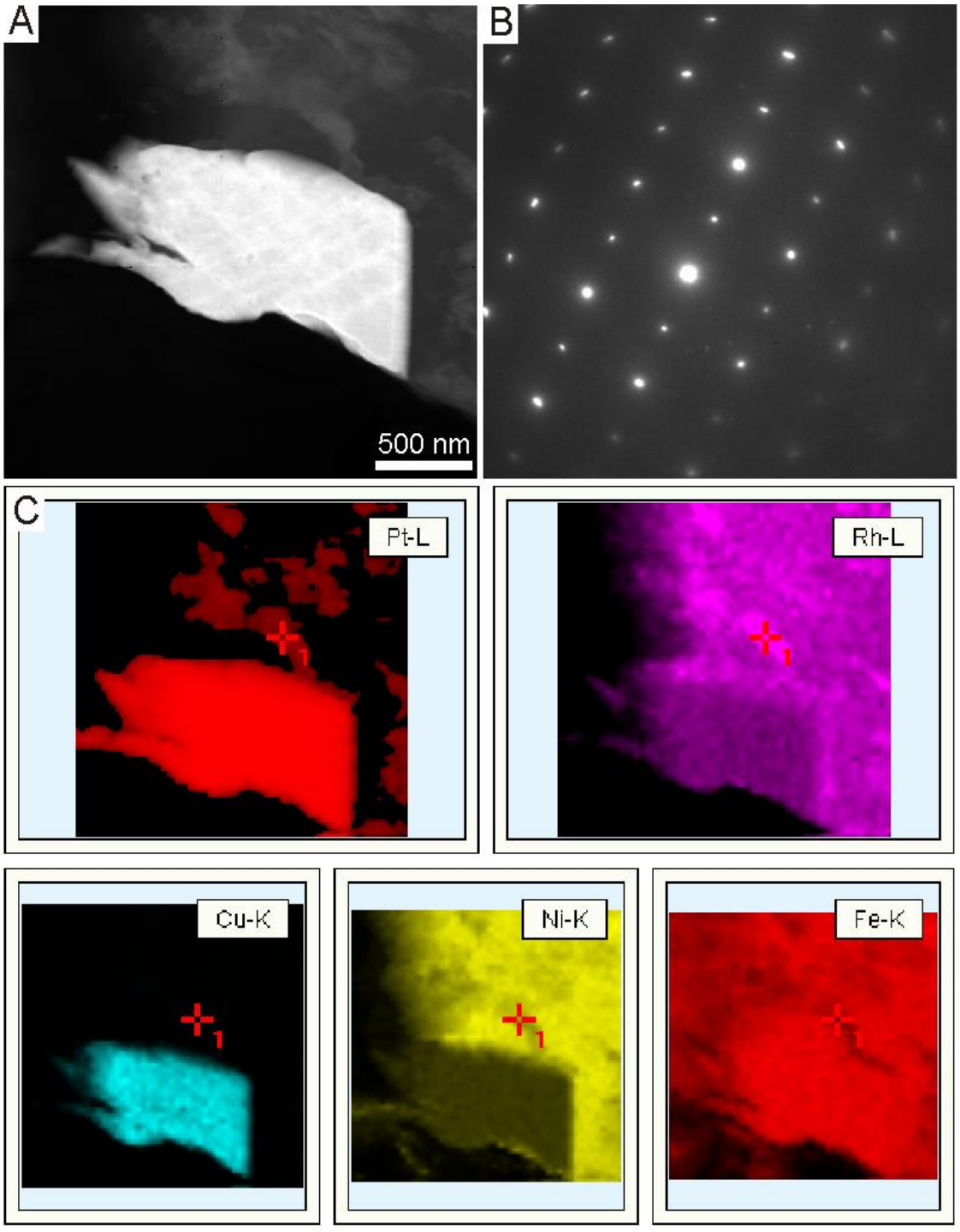

661

662 Fig 4

663

664

665

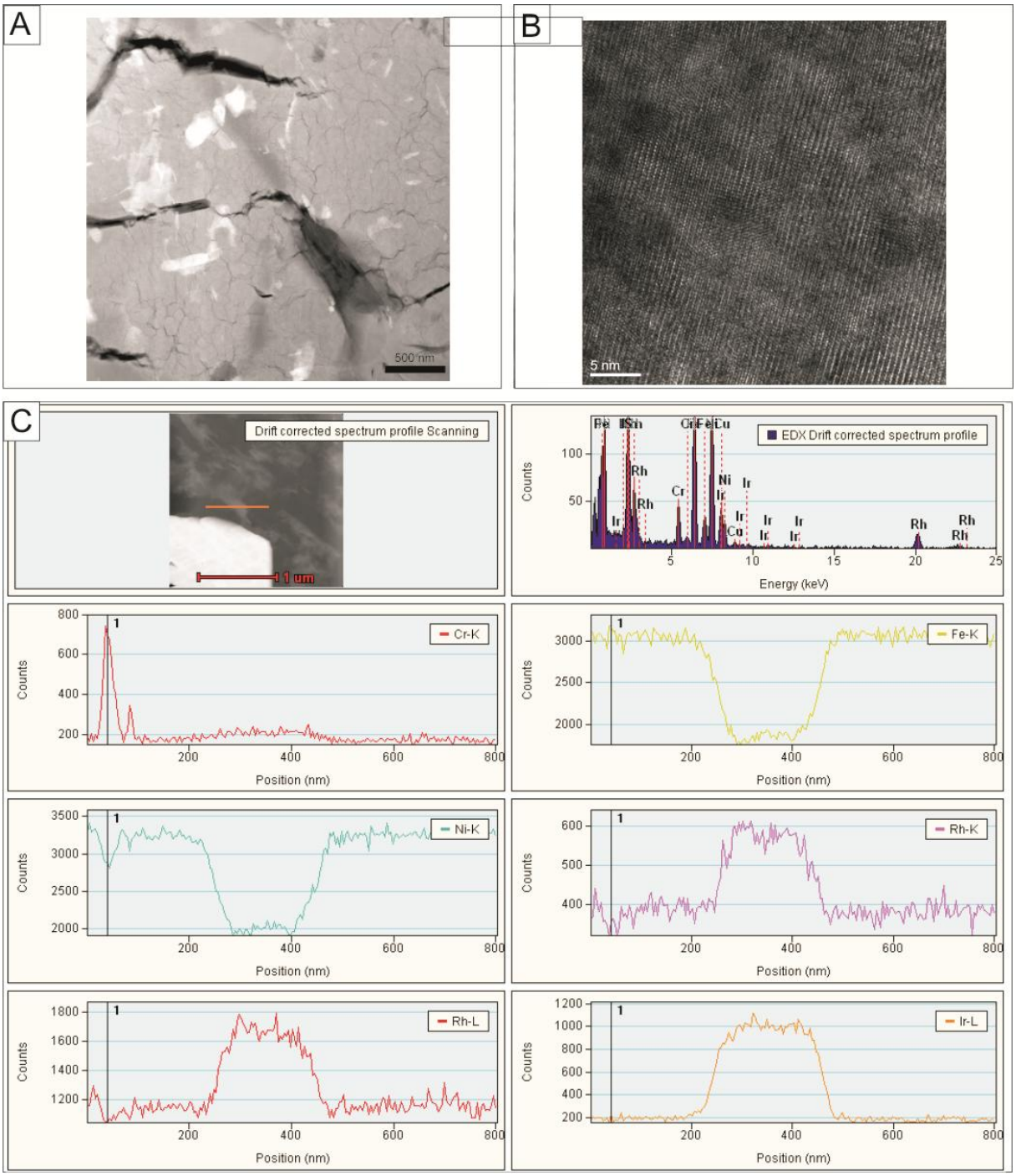

666

667

668 Fig 5

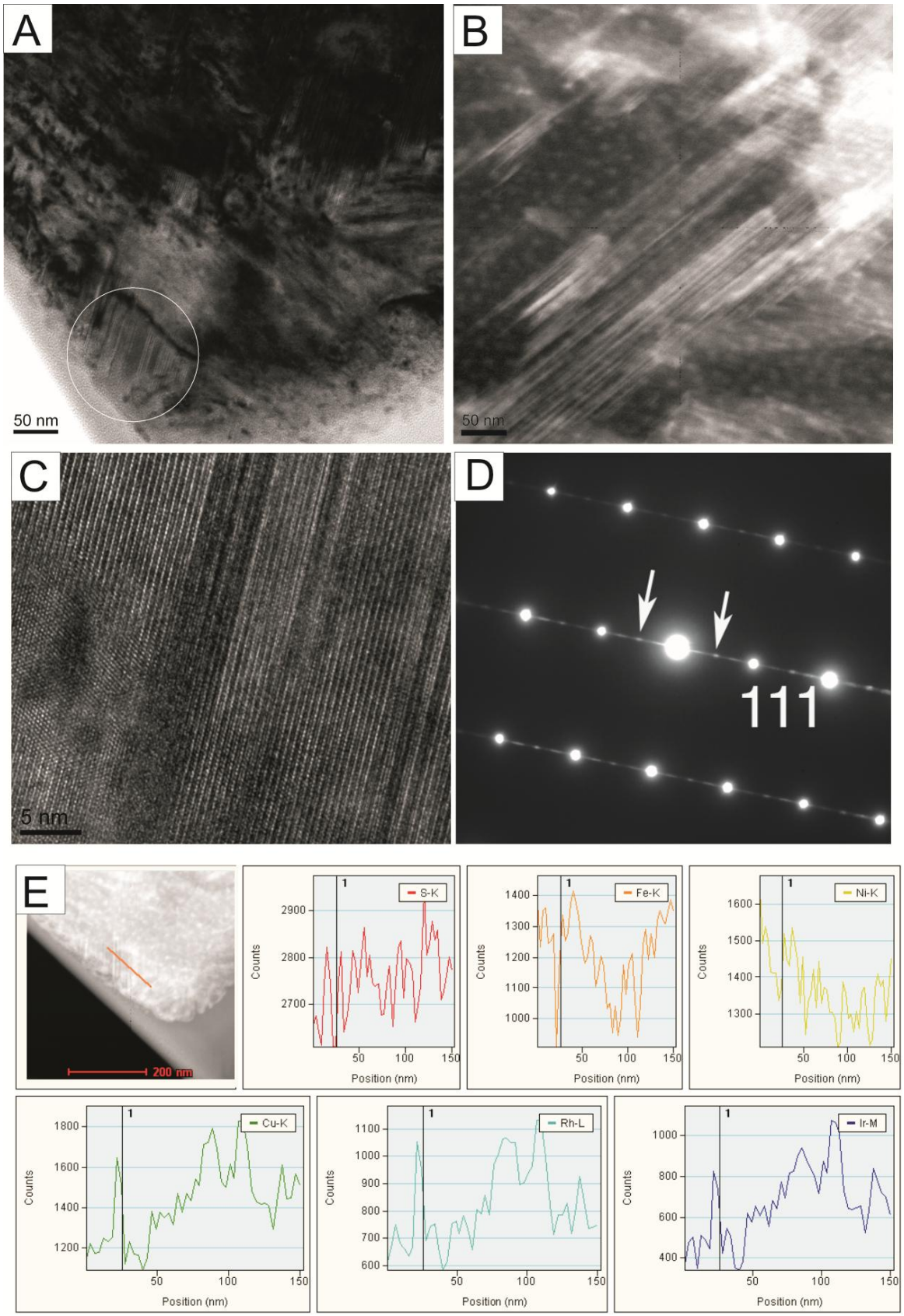

669

670 Fig 6

671

Table 1: EPMA measurements of Pd and Rh (in wt.%) from of the UG-2 (pn1_UG2 to pn3_UG2) and the Platreef (pn1_Pr to pn5_Pr) and LA-ICP-MS measurements of Pd and Rh (in wt.%) and Os, Ir, Ru and Pt (in ppm) in pentlandite from of the UG-2. Concentrations of Pd and Rh for the Platreef are mean values of n-analyses. Values "<" represent detection limits.

		EPMA		**LA-ICP-MS**						
		[wt.%]		[wt.%]		[ppm]				foils
		Pd	Rh	Pd	Rh	Os	Ir	Ru	Pt	
pn1_UG2		0.65	3.00	0.42	2.18	<1.1	327	3.94	<0.76	#3510
		0.63	2.35	0.65	2.38	<1.4	326	<1.2	1.44	
pn2_UG2		0.02	12.5	-	-	-	-	-	-	#3512,#3516,#3534
		0.05	10.3	-	-	-	-	-	-	
pn3_UG2		0.99	1.38	0.93	1.64	<0.3	471	1.53	3.52	#3514,#3523,#3533
		1.26	1.16	0.50	0.95	0.715	396	1.60	6.47	
		0.87	1.31	-	-	-	-	-	-	
	[n]	[ppm]								
pn1_Pr	5	680	<135	-	-	-	-	-	-	#3502, #3511
pn2_Pr	3	504	<136	-	-	-	-	-	-	#3504, #3509
pn3_Pr	4	360	<135	-	-	-	-	-	-	#3522
pn4_Pr	4	370	<135	-	-	-	-	-	-	#3524
pn5_Pr	4	357	<136	-	-	-	-	-	-	#3503

679 Table 2: Platinum-group mineral inclusions and PGE incorporation in pentlandite from the UG-2
680 chromitite and the Platreef. In the foils of the Platreef , no patchy solid solution of any PGE was
681 detected.

foil	sample no.	nPGM	grain size	remarks
		Platreef		
		AS10340		
#3502	pn1_Pr	PtTe	~50 nm	fluid inclusion trail
#3511	pn1_Pr	n.d.		
#3504	pn2_Pr	(Pt,Pd)Sn	~50 nm	unorientated relative to host sulfide
#3509	pn2_Pr	n.d.		
		AS7368		
#3522	pn3_Pr	Pt-(Fe,Cu)	~ 1µm	
#3524	pn4_Pr	Pt-(Fe,Cu)	200 nm	
#3503	pn5_Pr	PtBi	~50 nm	
		AS7372		
#3501	pn6_Pr	n.d.		
		UG-2 chromitite		
		AS8918b		
#3510	pn1_UG2	n.d.		patchy solid solution of Rh + Ir
#3512	pn2_UG2	Pt-(Fe,Cu)	~750 nm	patchy solid solution of Rh + Ir
#3516	pn2_UG2	PdSn	~50 nm	patchy solid solution and lamellae of Rh + Ir
#3534	pn2_UG2	n.d.		patchy solid solution of Rh + Ir
#3514	pn3_UG2	n.d.		patchy solid solution of Rh + Ir
#3523	pn3_UG2	n.d.		patchy solid solution of Rh + Ir
#3533	pn3_UG2	Pt-(Fe,Cu)	<50 nm	patchy solid solution of Rh + Ir

682

683

684